How to cite: Angew. Chem. Int. Ed. 2024, e202415949
doi.org/10.1002/anie.202415949

Perovskite Solar Cells Hot Paper

Revealing and Inhibiting the Facet-related Ion Migration for Efficient and Stable Perovskite Solar Cells

*Shujie Qu[#], Hao Huang[#], Jinhui Wang, Peng Cui, Yiyi Li, Min Wang, Liang Li, Fu Yang, Changxu Sun, Qiang Zhang, Pengkun Zhu, Yi Wang, and Meicheng Li**

Abstract: Ion migration is a major issue hindering the long-term stability of perovskite solar cells (PSCs). As an intrinsic characteristic of metal halide perovskite materials, ion migration is closely related to the atomic arrangement and coordination, which are the basic characteristic differences among various facets. Herein, we report the facet-related ion migration, and then achieve the inhibition of ion migration in perovskite through finely modulating the facet orientation. We show that the (100) facet is substantially more vulnerable to cationic migration than the (111) facet. The main reason for this difference in migration is that the cationic migration route in the (111) facet deviates from that in the (100) facet, which increases the active migration energy and weakens the contribution from the electric field during operation. We prepare a (111)-dominated perovskite film by incorporating a facile and green addition of water (H_2O) into the antisolvent, further achieving a power conversion efficiency (PCE) of 26.0 % (25.4 % certification) on regular planar PSCs and 25.8 % on inverted PSCs. Moreover, the unencapsulated PSCs can maintain 95 % of their initial PCE after 3500-hours operation under simulated AM1.5 illumination at the maximum power point.

Introduction

Metal halide perovskite solar cells (PSCs) have achieved substantial advances in power conversion efficiency (PCE), with a certified PCE reaching 26 % for single-junction devices and 29.0 % for perovskite/perovskite tandem devices, showing great potential for commercialization.[1] However, the vital prerequisite for the commercialization of these high-efficiency PSCs is long-term stability. Currently, most efficient PSCs with a PCE > 25 % are based on $FAPbI_3$-dominated materials.[2] As an ionic crystal compound, this perovskite material undergoes ion migration, which must be urgently addressed to enhance the stability of efficient PSCs.

Many studies have been reported from theoretical and experimental perspectives on understanding and inhibiting the ion migration of PSCs.[3] In general, organic possess low activation energies for migration (generally < 1 eV), resulting in this ion migrating through defects and grain boundaries at room temperature and in nonoperating states.[4] Under heat, light and electric field conditions, the inevitable conditions that PSCs face during operation increase the severity of ion migration. Considering the impact of ion migration on PSC stability, many scholars have reported many inhibition strategies, such as component engineering, additive engineering, and layer blocking.[5] Although these researchers have made considerable advances in ion migration inhibition, mobile ions are likely to be controlled externally. Undoubtedly, a comprehensive understanding of ion migration behavior and kinetics is necessary to develop the best-performing PSCs with high intrinsic stabilities.

As a polycrystalline film, perovskite films are composed of various crystal facets. Different crystal facets have distinct electronic and physical properties due to their unique atomic arrangement and coordination characteristics, subsequently leading to each facet responding differently to external conditions. For example, the (220) facet of methylammonium lead iodide ($MAPbI_3$) exhibits relatively high electron and hole conductivities.[6] Conversely, the (112) facet shows greater ionic conductance than the (100) facet.[7] It was also reported that both (100) and (111) facets exhibit higher carrier mobility and lower defect state density compared to the (110) facet, and (111)-dominated perovskite films demonstrate electron-dominant traps, (100)-dominated perovskite films show hole-dominant traps.[8] In 2023, Ma *et al.* revealed that perovskite degradation kinetics differ for various facets and confirmed that the (100) facet is substantially more unstable in moisture-induced degradation than the (111) facet.[9] However, as an external factor, moisture can be effectively blocked by encapsulation during the practical operation of PSCs. The intrinsic stability without the influences of additives or environments arises mainly due to ion migration. Ion migration is supposed to

[*] S. Qu,[#] H. Huang,[#] J. Wang, P. Cui, M. Wang, L. Li, F. Yang, C. Sun, Q. Zhang, P. Zhu, M. Li
State Key Laboratory of Alternate Electrical Power System with Renewable Energy Sources
North China Electric Power University
Beijing 102206, China
E-mail: mcli@ncepu.edu.cn
Y. Li, Y. Wang
Key Laboratory of Advanced Light Conversion Materials and Biophotonics
School of Chemistry and Life Resources Institution
Renmin University of China
Beijing 100872, China
[#] These authors contributed equally

suffer from different migration kinetics at various facets due to differences in the ion arrangement and coordination characteristics. This potential relation between facet and ion migration provides a novel approach for expanding the insight into ion migration behavior. Therefore, it is valuable to conduct in-depth research on inhibiting ion migration from a perspective of crystal facet for realizing efficient PSCs with excellent intrinsic stability.

Herein, we reveal the characteristics of ion migration on different facet and discover the underlying mechanisms, and achieve migration inhibition by modulating crystal facet. We find that the (100) facet is substantially more vulnerable to ion migration than the (111) facet through *in situ* measurements and novelly designed measurements. By combining theory calculations and experiments, we confirm that the cation is the main component that shows different migration behaviors and clarify the underlying reason for this difference. The cationic migration route in the (111) facet deviates from that in the (100) facet, which increases the active migration energy and weakens the contribution from the electric field during operation. We proposed a simple strategy of antisolvent engineering to finely modulate the crystal facet, leading to a PCE of 26.0 % (25.4 % certification) on TiO_2-based planar PSCs with the (111)-dominated film. Moreover, the PSCs maintain approximately 95 % of their initial PCE after continuous operation under simulated AM1.5 illumination at the maximum power point for 3500 h.

Results and Discussion

Modulating Crystal Facet and the Photovoltaic Performance of PSCs

To obtain a detailed understanding of the ion migration behaviours on different perovskite facets, perovskite films dominated by different facets had to be prepared first. To date, most perovskite films applied in efficient PSCs were (100)-dominated, and they served as the normal samples in this work. By incorporating a facile and green additive of water (H_2O) into an antisolvent, we prepared a (111)-dominated perovskite film with optmized surface mopgology, as evidenced by X-ray diffraction (XRD) measurement (Figure 1a) and atomic force microscopy (AFM) measurement (Supplementary Figure S1, Supplementary Note 1).[10] Notably, in the following discussion, the (111)-dominated perovskite film and the corresponding device were labelled the target sample. To directly show the transformation from a (100)-dominated film to a (111)-dominated film, we calculated the peak ratio of (111)/(100), and the results are shown in Figure 1b. For the target film, the peak ratio of (111)/(100) was 4.1, which was approximately seven times larger than that of the normal film: 0.6.[11] The (111)-dominated film with a high ratio of (111)/(100) was reproduced by a batch of repeatable experiments with 10 samples (Figure 1b and Figure S2). These results confirmed that the H_2O additive in the antisolvent could finely obtain perovskite films with well-oriented facets, providing an experimental basis for investigating ion migration on different facets. A schematic diagram of the (100) and (111) facets was proposed to show the atomic arrangement (Figure 1c). On the (100) facet, the metal cations (Pb) or organic cations (FA) were connected to I anions with Pb–I or FA–I layer terminations. The (111) facet was terminated by 3/8 FA cations and 3/2 I anions, and the unsaturated bond of the I anions was balanced by either FA or Pb cations at the corresponding crystallographic sites. These different ion arrangements should be the origin of the differences in ion migration behaviour that we discussed in detail in this work.

To explain the reason for the (111)-oriented crystallization of the perovskite film, we first analysed the film formation process. In our experiments, perovskite films were fabricated by one-step spin-coating using ether as an antisolvent. After spin-coating, the perovskite film was first pre-annealed for 3 min at 60 °C and then annealed for 15 min at 130 °C. We characterized the pre-annealed perovskite by XRD and found that the pre-annealed normal and target films exhibited facet orientations similar to those of their corresponding annealed films, indicating that the H_2O incorporated in the antisolvent influenced perovskite crystallization at an early stage, possibly through nucleation (Figure S3). Density functional theory (DFT) calculations were applied to determine the absorption energies of H_2O molecules on the (100), (110) and (111) facets, as demonstrated by the XRD results.[12] The DFT results indicated that the (111) facet was the most difficult to absorb, followed by the (110) facet, and the (100) facet was the easiest to absorb (Figure S4 and 5). These results indicated that the incorporated H_2O was first preferentially absorbed on the (100) facet and then on the (110) facet, and the (111) facet was unabsorbed. According to the traditional Kossel model of crystallization, when the formed nucleus acquired the characteristics of a facet under continuous nucleation, the absorbed impurity inhibited facet formation through atom assembly from the surrounding environment. In this work, when the nucleus was ready to form the (100) facet, the absorbed H_2O molecules inhibited atom assembly, thereby inhibiting the growth of the (100) facet (Figure S6). H_2O interference during perovskite nucleation caused the unabsorbed (111) facet to become the predominant growth orientation, leading to a (111)-dominated perovskite film.

After we prepared perovskite films with well-oriented facets, we characterized their photoelectric properties and the photovoltaic performance of the corresponding PSCs. The ultraviolet (UV) visible (vis) absorption, photoluminescence (PL) and time-resolved photoluminescence (TRPL) spectra demonstrated that the normal and target films showed excellent photoelectric properties and good spatial uniformity (Figure 1d and 1e, Figure S7).[13] Specifically, the fitted carrier lifetime of the target film was 1089 ns, slightly longer than that (1044 ns) of control film (Figure 1e), indicating the reduced non-radiative recombination that can also be demonstrated by the reduced defect density (Figure S8, Supplementary Note 2). After determining the optimal amount of water that incorporated into antisolvent (Figure S9, Supplementary Note 3), we fabricated planar PSCs structured as fluorine-doped tin oxide (FTO)/com-

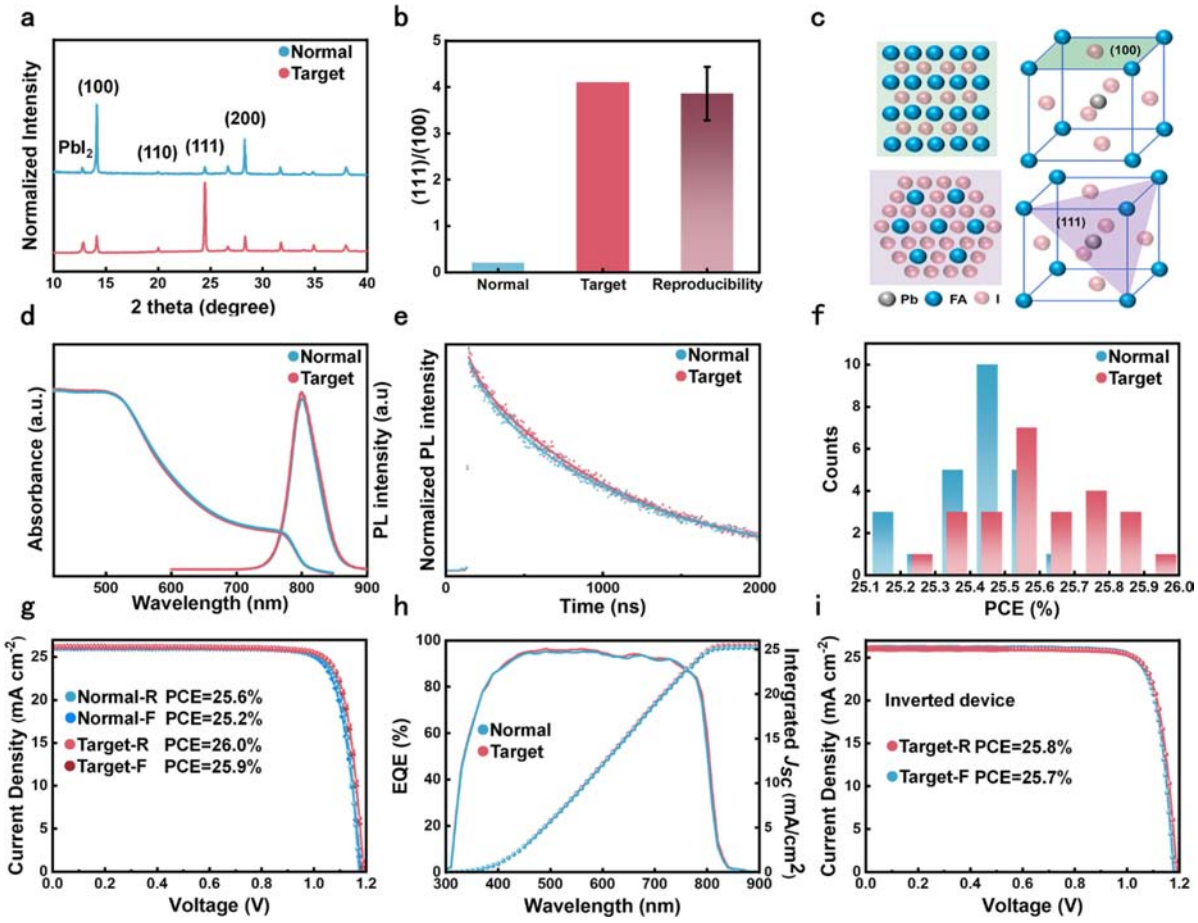

Figure 1. **Perovskite films with well-oriented facets and their photovoltaic performance**. (a) XRD spectra of the normal and target films. (b) Peak intensity ratio of (111)/(100). (c) Schematic diagram of the (100) and (111) facets. (d) Absorption and PL spectra of the perovskite films. (e) TRPL spectra of perovskite films. (f) Distribution histograms of the PCE values of the 25 normal and target PSCs. (g) J–V curves of normal and target PSCs with an active area of 0.08 cm^2. (h) External quantum efficiency (EQE) spectra of the normal and target PSCs. (i) Reverse J–V curves of the inverted target PSC with an active area of 0.08 cm^2; the device structure was FTO/Me-4PACz/perovskite/PEACl/C60/BCP/Ag.

pact-titanium dioxide (c-TiO_2)/perovskite/methoxy-phenethyl ammonium iodide (MeO-PEAI)/ 2,2′,7,7′-tetrakis [N, N-di(4-methoxyphenyl) amino]-9-9′-spirobifluorene (Spiro-OMeTAD)/gold (Au) and characterized their photovoltaic performance. Figure 1f shows the PCE distribution of a batch of normal and target PSCs, where the average PCE of the target PSC was 25.6 %, which was slightly greater than that of the normal PSC (25.4 %). This slightly improved PCE should result from the reduced non-radiative recombination due to the reduced defect of target perovskite film (Figure S10 and Figure 11). Impressively, the target PSCs achieved a maximum PCE of 26.0 %, with a short-circuit current density (J_{sc}) of 26.21 mA/cm^2, an open-circuit voltage (V_{oc}) of 1.187 V and a fill factor (FF) of 83.44 %. In comparison, the normal PSCs achieved a champion PCE of 25.6 %, with a J_{sc} of 26.11 mA/cm^2, a V_{oc} of 1.174 V and an FF of 83.39 %. The corresponding external quantum efficiency spectra shown in Figure 1h indicated that the integrated J_{sc} values of the normal and target PSCs showed small variations from the values obtained from *J–V* measurements. Notably, one of our best-performing target PSCs was validated by a third-party institute of the National Institute of Metrology with a certified PCE of 25.4 % (Figure S12). Although the (111) facet has attracted the interest of researchers in recent years due to its high humidity resistance, (111)-dominated perovskite films have rarely been applied to fabricate high-efficiency PSCs. We first achieved a PCE of 26 % based on a (111)-dominated perovskite film, which was supposed to significantly promote the achievement of high-efficiency and stable PSCs. The excellent applicability of the (111)-dominated perovskite film in high-efficiency PSCs was demonstrated by a device with a large aperture area of 1 cm^2 and an inverted structure (FTO/[4-(3,6-dimethyl-9H-carbazol-9-yl) butyl] phosphonic acid (Me-4PACz)/perovskite/phenethyl ammonium chloride (PEACl)/carbon-60 (C_{60})/ 2,9-dimethyl-4,7-diphenyl-1,10-phenanthroline (BCP)/silver (Ag)). The 1 cm^2 PSCs achieved a PCE of 24.1 % (Figure S13 and Supporting Information Table 2). Besides, the target inverted PSCs possessed good repeatability (Figure 1i and Supporting Information Table 3, 4), and achieved a champion PCE of 25.8 %, with a J_{sc} of 26.10 mA/cm^2, a V_{oc} of 1.187 V and an FF of 83.31 %.

Facet-related Ion Migration

We revealed the facet-related ion migration behavior of the prepared perovskite film with well-oriented facets. We carried out optical microscopy to observe ion migration in perovskite films *in situ* under an applied external field in lateral structures (a schematic of the measurements is shown in Figure S14). As shown in Figure 2a, the normal and target films were uniform in the initial stage. A white strip on the anode side clearly emerged in the normal film after aging for 70 s.[14] The white strip that grew was attributed to the FA-poor perovskite resulting from ion migration under an external field. In comparison, the target film was still uniform without obvious changes in the region near the anode side. As the time increased to 120 s, the width of the emerged white strip in the normal film increased, indicating that the film continually underwent ion migration. However, the target film could remain uniform, suggesting that there was negligible ion migration. These intuitive results indicated a large difference in the ion migration behaviors of perovskite films with different facets. The ion migration characteristics in PSCs with different films were characterized. First, we monitored the electroluminescence of the PSCs to evaluate the ion migration. The electroluminescence came from the radiative recombination of injected electrons and holes, which was strongly influenced by nonradiative recombination.[15] Ion migration could induce defects and reshape the defect distribution, which increased nonradiative recombination, resulting in losses of injected electrons and holes. As shown in Figure 2b and 2c, at the initial stage, both PSCs showed a high-intensity electroluminescence peak, indicating that these PSCs possessed similar excellent photoelectric properties. This finding was consistent with the results of the *J–V* curves. However, as time increased, the electroluminescence intensity of the normal PSCs quickly decreased, which resulted from the increase in ion migration and increased nonradiative recombination. In comparison, the electroluminescence intensity of the target PSCs slightly decreased, which was apparently more stable than that of normal PSCs, indicating largely mitigated ion migration. Since ion migration was closely related to the carrier dynamics in PSCs, we characterized the ion migration in PSCs by capturing the real-time PL response to an applied external electric field

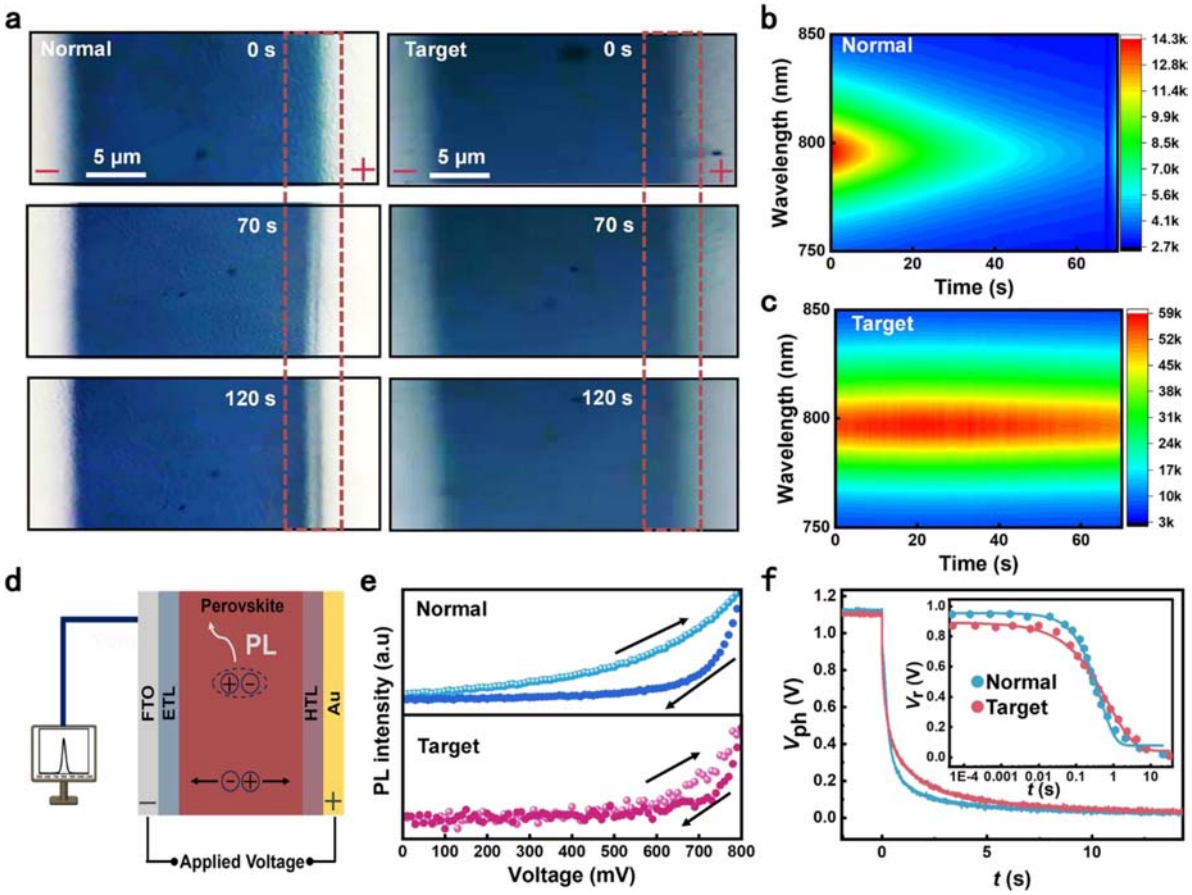

Figure 2. **Observation of facet-related ion migration**. (a) In situ optical microscopy images of normal and target films. The perovskite films were under a bias voltage of 0.5 V/μm, and before testing, the films were aged under simulated 1.5G illumination for 5 h under ambient conditions at 40% RH and 25 °C. (b, c) In situ electroluminescence mapping of normal and target PSCs under a bias voltage of 2 V, conducted under ambient conditions with 35% RH and 25 °C. (d) Schematic diagram of the PL–V hysteresis test. (e) PL–V curves of the normal and target PSCs. (f) OCVD curves of the normal and target PSCs.

(E_{ex}), i.e., PL–V hysteresis. We designed a novel test system by combining PL measurements with electrochemical impedance spectroscopy (EIS); the former technique was used to obtain the PL information, and the latter technique was used to finely normalize the applied voltage (Figure 2e). E_{ex} had multiple effects on the photoexcited carrier dynamics. First, the E_{ex} directly changed the drift velocity of the carrier by changing the practical electric field within the PSCs. Second, the E_{ex} could induce ion migration, resulting in defect formation and redistribution. Compared to the obvious PL–V hysteresis in normal PSCs, that in the target PSCs was much smaller. The PL intensity instantly responded to the carrier dynamics, which were not responsible for the PL–V hysteresis. The relatively slow kinetics of ion migration on the time scale could explain this difference. Hence, the reduced PL–V hysteresis was associated with mitigated ion migration in the target PSCs. To gain further insights into the kinetics of ion migration, we conducted open-circuit photovoltage decay (OCVD) and circuit-switch transient photoelectric technique (cs-TPT) studies, as shown in Figure 2f.[16] The OCVD profiles consisted of a rapid component that decayed within a few milliseconds and a very gradual component that extended to tens of seconds; these components were linked with charge recombination and ion migration, respectively.[17] The notably reduced voltage decay of the target device was in excellent agreement with the mitigated ion migration. The inset of Figure 2f presents the variation in the ion accumulation-induced photovoltage (V_r) as a function of time (t) derived from the cs-TPT data (see detailed analysis in the SI). In brief, the V_r-t plots could be effectively fitted to the Kohlrausch function (details shown in Supplementary Note 4), $V_r(t) = V_m \times \exp\left[-\left(\frac{t_{ex}}{\tau}\right)^{\beta}\right]$, where V_m and β are constants and τ is the time constant of ion migration.[18] The τ value of the target PSCs (~0.74 s) was approximately 70 % larger than that of the normal PSCs (~0.43 s), validating the effective inhibition of ion migration in the target PSCs. Overall, although the perovskite films were dominated by different facets and the corresponding PSCs showed similar photoelectric properties, including carrier dynamics and photovoltaic performance, the ion migration behaviors in these films and the corresponding PSCs were significantly different. This result demonstrated that ion migration was directly associated with the crystal facets, and the (100) facet is substantially more vulnerable to cationic migration than the (111) facet.

After clarifying the ion migration characteristics in different facet, we focused on the specific characteristics of the ion migration behavior. In short, we investigated which ions exhibited different migration kinetics and the corresponding reasons. First, to clarify the type of mobile ions, Kelvin probe force microscopy (KPFM) and time-of-flight secondary ion mass spectrometry (TOF-SIMS) were carried out.[19] As discussed previously, lateral ion migration could lead to a nonuniform ion distribution on both sides of the perovskite film. According to the self-doping characteristics of perovskites, the accumulation of FA^+ vacancies should result in p-type doping, and the accumulation of FA^+ ions should result in n-type doping. Self-doping by the redistribution of FA^+ under an external field could induce changes in the film surface potential, as characterized by Kelvin probe microscopy (Figure S15, Figure 3a, Figure S16). The KPFM image of the normal film exhibited obvious lateral gradient changes in the surface potential, suggesting a nonuniform distribution of FA^+. Specifically, the surface potential continued to increase from the region near the cathode to the region near the anode, which was consistent with the assumption that p-doping occurred near the anode. Similar to the optical image, the KPFM image of the target film exhibited a uniform distribution of surface potential throughout the region, demonstrating that the ion migration that could induce self-doping of perovskite was negligible in the target film. To determine the difference in FA^+ migration, TOF-SIMS was carried out on normal and target PSCs aged under simulated 1.5G illumination for 12 h under ambient conditions at 40 % relative humidity (RH) and 25 °C. The results of TOF-SIMS demonstrated that FA^+ ion migration in normal PSCs was more severe than that in target PSCs, which was consistent with the results of KPFM measurements (Figure 3b). We fabricated a $MAPbI_3$ film with well-oriented facets to validate the facet-independent ion migration phenomenon, considering the presence of severe MA^+ migration. Figure S17a shows that our approach of incorporating H_2O into an antisolvent to obtain a (111)-dominated perovskite could be applied to $MAPbI_3$. The PL–V results (Figure S17b) validated the obvious difference in ion migration between the normal and target MA-based PSCs, and the TOF-SIMS results (Figure S17c) proved that the reduced ion migration in the target MA-based PSCs mainly resulted from the mitigation of MA^+ migration.

To determine the reason for the difference in cationic migration between the (111) facet and (100) facet, we investigated the facet plane structure and the atomic arrangement. As shown in Figure 3c, FA^+ was arranged in an adjacent and parallel manner in the (111) and (100) facets, which could provide a direct route for migration, especially for cation vacancies. In the (100) facet, the arrangement of FA^+ was vertical and parallel to the substrate, making the FA^+ migration route vertical and parallel to the substrate. In comparison, the arrangement of FA^+ in the (111) facet was inclined toward the substrate, which caused the FA^+ migration route to incline toward the substrate. This migration route in (111) could weaken the contribution from the built-in electric field. This weakened field was beneficial for reducing ion migration when PSCs were continuously operating or under an applied voltage. In addition to the migration direction, the different atomic arrangements were supposed to influence the migration activation energy of FA^+ since the surroundings of FA^+ were different. We carried out DFT calculations to obtain the migration activation energy of FA^+ in the (100) and (111) facets (Figure 3d). The migration activation energy of FA^+ in the (111) facet was obviously greater than that in the (100) facet, which could support the suppressed ion migration in the (111)-dominated perovskite film. The increased active migration energy was validated by experimental

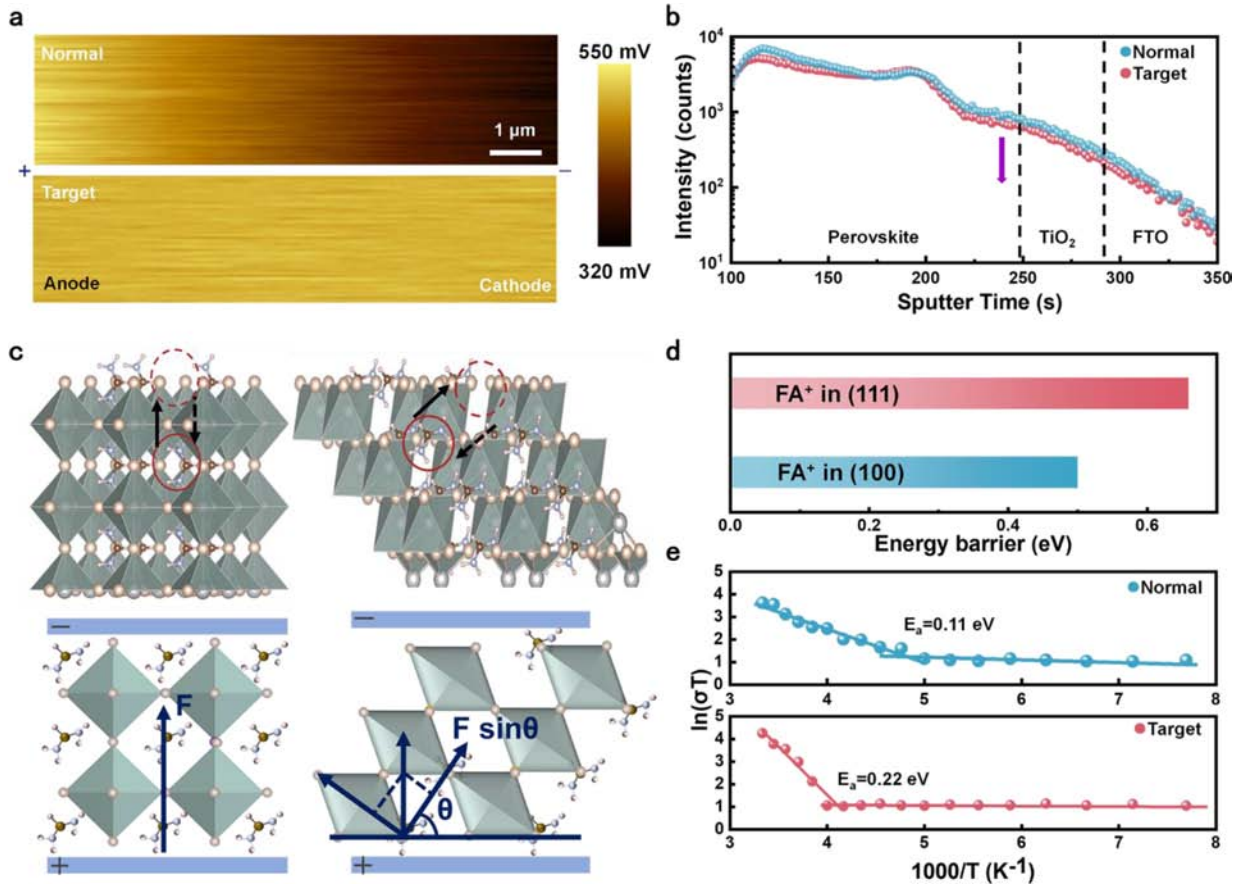

Figure 3. **Mechanism of facet-related ion migration**. (a) KPFM images of normal and target films. (b) TOF-SIMS spectra of normal PSCs aged under simulated 1.5G illumination for 12 h under ambient conditions at 40% RH and 25 °C. (c) Schematic diagram of the cationic migration route in the (100) and (111) facets. (d) Active migration energy of cationic migration in the (100) and (111) facets. (e) Temperature-dependent conductivity measurements of normal and target perovskite films under ambient conditions with 35% RH and 25 °C.

measurements through capturing the temperature-dependent conductivity of the normal and target films (Figure 3e). The ion active migration energy in the target film was 0.22 eV, which was twice that (0.11 eV) of the normal film.[20] The increased active migration energy demonstrated by the DFT calculations and experimental measurements could intrinsically explain why ion migration was more difficult in the (111) facet than in the (100) facet. Hence, the cationic migration in perovskite films was closely related to the facet, which mainly resulted from the different migration routes. The ion migration in the (111) facet was more energy-consuming, making the (111) facet intrinsically more stable than the (100) facet. In addition, the effect of migration mitigation should be further amplified when PSCs were in an operation state since the migration direction in the (111) direction could weaken the contribution from the electric field within the PSCs.

Enhanced Device Stability

The (111) facet was proven to possess higher humidity resistance and less ion migration than the (100) facet, which was beneficial for fabricating stable PSCs using (111)-dominated perovskite films. To systematically evaluate the stability of perovskite films dominated by different facets and the stability of the corresponding PSCs, we carried out a series of measurements. First, we characterized the humidity stability of the perovskite films by placing them under ambient conditions with a RH of 45% for 3000 h. We characterized the film properties at the initial and final stages using XRD measurements. For the normal film, the intensity of the (100) peak strongly decreased, accompanied by an increase in the intensity of the PbI_2 peak after aging for 3000 h, indicating that the perovskite film decomposed under humid conditions. In comparison, the XRD pattern of the target film showed only slight changes (Figure 4a). The PL spectra (Figure 4b) and O 1 s spectra (Figure S18) of the normal and target films before and after aging proved that the target film possessed high humidity stability. Harsh conditions of 85% RH were applied to evaluate the humidity stability of the perovskite films. Both the PL and XRD results proved that the target film possessed high humidity stability (Figure S19 and Figure S20). We evaluated the light stability of perovskite films by placing them under UV irradiation in a N_2 glovebox, which could reflect the influence of ion migration on film stability. As shown in Figure 4c, after aging for 1500 h, the (100) peak in the

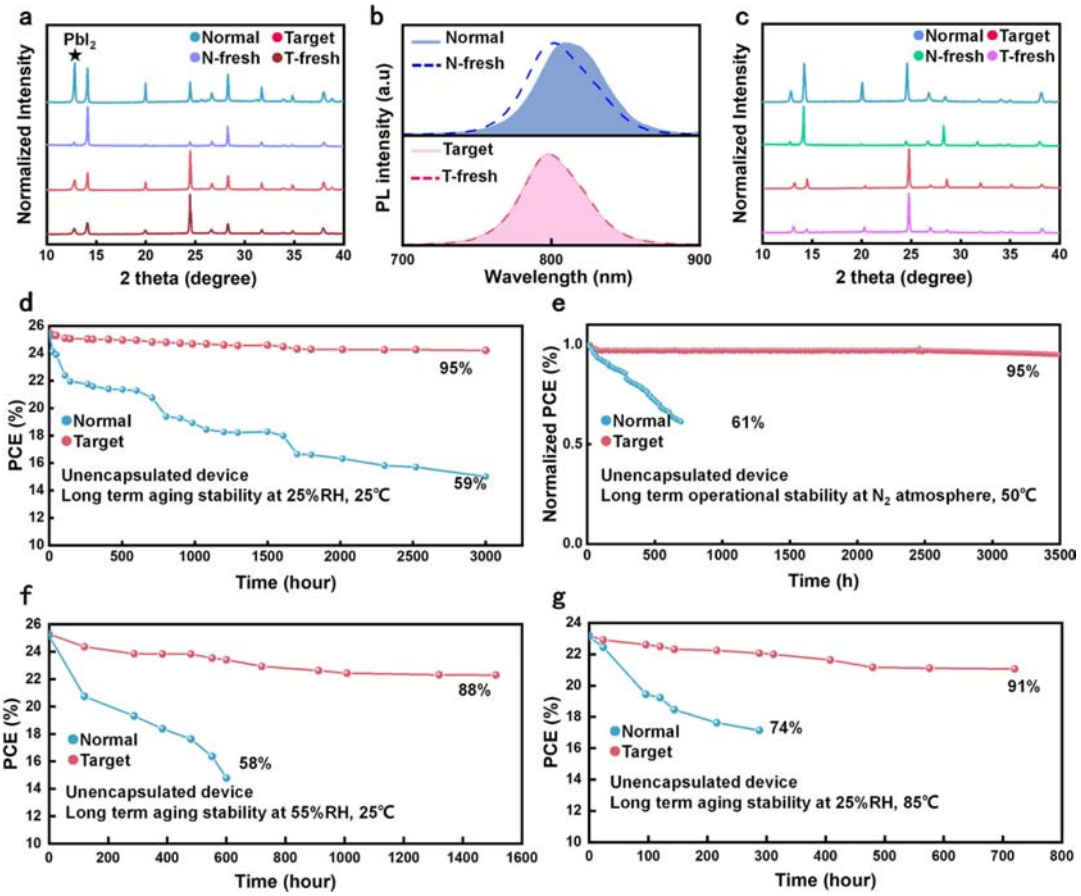

Figure 4. **Accelerated stability tests**. (a) XRD and (b) PL spectra of the normal and target films. Both films were stored under ambient conditions with a RH of 45 % for 3000 h. (c) XRD patterns of the normal and target films; both films were stored under UV irradiation for 1500 h. (d) Long-term stability of unencapsulated devices stored under ambient conditions of 25 % RH and 25 °C. (e) Operational stability of the unencapsulated devices under continuous simulated AM1.5 illumination at the maximum power point and at approximately 50 °C in a N2 glove box. (f) Long-term stability of unencapsulated devices stored under ambient conditions of 55 % RH and 25 °C. (g) Long-term stability of unencapsulated devices stored under ambient conditions of 25 % RH and 85 °C.

normal film clearly decreased, and the PbI_2 peak clearly increased. In comparison, the (111) peak in both the normal and target films slightly changed, which demonstrated that the (111) facet was more stable than the (100) facet. The enhanced light stability of the (111) facet resulted from reduced migration under UV radiation.

After discussing the enhanced stability of the target film, we characterized the device stability. We monitored the PCE evolution of unencapsulated devices stored under ambient conditions (25 % RH, 25 °C). The target device could maintain 95 % of its initial PCE after aging for 3000 h, while the normal device could maintain 59 % of its initial PCE (Figure 4d). We measured the long-term operational stability of unencapsulated devices under continuous 1-sun illumination conditions in a N_2 glovebox (Figure 4e). Impressively, the target device could maintain 95 % of its initial PCE after operating for 3500 h, while the normal PSCs obviously decreased after 500 h.[21] Extreme conditions were applied to the device to evaluate its stability. First, we increased the humidity to 55 % RH and found that the target device could maintain 88 % of its initial PCE after storage for 1512 h, while the PCE of the normal device quickly decayed to 58 % of its initial PCE after storage for 600 h (Figure 4f). In addition, the encapsulated target device could maintain 92 % of its initial PCE after storage for 1416 h under 85 % RH, showing better stability than that of the normal device (Figure S21). Second, a high temperature of 85 °C was applied to the device to characterize its heat durability. As shown in Figure 4g, the target device could maintain 91 % of its initial PCE after storage at 25 % RH and 85 °C for 720 h. In contrast, the normal device decayed to 74 % of its initial PCE in at most 300 h. From the measurements and discussion of the film and device stability, we found that the target film and PSCs showed enhanced storage and operational stability, which mainly resulted from the (111) facet possessing high humidity resistance and reduced ion migration, which was an intrinsic factor in determining device stability. The clarification on ion migration from a perspective of facet, and the proposed facet modulation approach with excellent extendibility (Figure S22 and Supplementary Note 5) should provide new idea for enhancing the stability of high-efficiency devices.

Conclusions

In summary, we reported that cationic migration is closely related to the crystal facets of perovskite films and inhibited ion migration by modulating crystal facet. The (100) facet is substantially more vulnerable to cationic migration than the (111) facet, which mainly results from the cationic migration route in the (111) facet deviating from that in the (100) facet. Based on the (111)-dominated perovskite film obtained by finely controlling the perovskite crystallization orientation, the TiO_2-based planar PSCs achieve a PCE of 26.0 % (25.4 % certification), which is the highest value among the PSCs based on the (111)-preferred film. Notably, the perovskite film and device exhibit enhanced stability under high-humidity and high-temperature conditions. The PSCs maintain approximately 95 % of their initial PCE after continuous operation under simulated AM1.5 illumination at the maximum power point and at approximately 50 °C for 3500 h. Our work provides new insight into ion migration and overcoming the bottleneck regarding perovskite stability from a novel perspective of crystal facet, providing more opportunities for promoting PSCs' commercialization.

Acknowledgements

S.Q., H.H. and M.L. conceived the idea. M.L., H.H. and P.C. guided the work as supervisors. S.Q. and H.H. did experimental designs, device fabrication, and data analysis. Y.L., Y.W. and F.Y. participated in the device fabrication and some characterizations. J.W. and M.W. conducted the DFT calculation and analysis. L.L. assisted with the EL spectra, active migration energy, and PL–V hysteresis test. P.C. and C.S. contributed to the ion migration characterization. S.Q. and H.H. wrote the first draft of the manuscript. F.Y., Q.Z., P. Z. and C.S. assisted in revision and polishing the manuscript language. All authors discussed the results and contributed to the revisions of the manuscript.

This work is supported partially by the Key Research and Development Program sponsored by the Ministry of Science and Technology (MOST) (Grant nos. 2022YFB4200301), National Natural Science Foundation of China (Grant nos. 52232008, 51972110, 52102245, 52072121, 52402254 and 22409061), Beijing Natural Science Foundation (2222076, 2222077), Beijing Nova Program (20220484016), Young Elite Scientists Sponsorship Program by CAST (2022QNRC001), 2022 Strategic Research Key Project of Science and Technology Commission of the Ministry of Education, Huaneng Group Headquarters Science and Technology Project (HNKJ20-H88), State Key Laboratory of Alternate Electrical Power System with Renewable Energy Sources (LAPS2024-05), the Fundamental Research Funds for the Central Universities (2022MS029, 2022MS02, 2022MS031, 2023MS042, 2023MS047) and the NCEPU "Double First-Class" Program.

Conflict of Interest

The authors declare no conflict of interest.

Data Availability Statement

The data that support the findings of this study are available from the corresponding author upon reasonable request.

Keywords: Perovskite solar cells · ion migration · crystal facet · stability

[1] a) Y. Rong, Y. Hu, A. Mei, H. Tan, M. I. Saidaminov, S. I. Seok, M. D. McGehee, E. H. Sargent, H. Han, *Science* **2018**, *361*, eaat8235; b) P. Shi, Y. Ding, B. Ding, Q. Xing, T. Kodalle, C. M. Sutter-Fella, I. Yavuz, C. Yao, W. Fan, J. Xu, Y. Tian, D. Gu, K. Zhao, S. Tan, X. Zhang, L. Yao, P. J. Dyson, J. L. Slack, D. Yang, J. Xue, M. K. Nazeeruddin, Y. Yang, R. Wang, *Nature* **2023**, *620*, 323–327; c) Y. Zhang, Q. Song, G. Liu, Y. Chen, Z. Guo, N. Li, X. Niu, Z. Qiu, W. Zhou, Z. Huang, C. Zhu, H. Zai, S. Ma, Y. Bai, Q. Chen, W. Huang, Q. Zhao, H. Zhou, *Nat. Photonics* **2023**, *17*, 1066–1073; d) C. Liu, Y. Yang, H. Chen, J. Xu, A. Liu, A. S. R. Bati, H. Zhu, L. Grater, S. S. Hadke, C. Huang, V. K. Sangwan, T. Cai, D. Shin, L. X. Chen, M. C. Hersam, C. A. Mirkin, B. Chen, M. G. Kanatzidis, E. H. Sargent, *Science* **2023**, *382*, 810–815; e) M. A. Green, E. D. Dunlop, M. Yoshita, N. Kopidakis, K. Bothe, G. Siefer, H. Hao, *Prog. Photovoltaics* **2023**, *31*, 651–663.

[2] a) C. Fei, N. Li, M. Wang, X. Wang, H. Gu, B. Chen, Z. Zhang, Z. Ni, H. Jiao, W. Xu, Z. Shi, Y. Yan, J. Huang, *Science* **2023**, *380*, 823–829; b) F. Zhang, S. Y. Park, C. Yao, H. Lu, S. P. Dunfield, C. Xiao, S. Uličná, X. Zhao, L. Du Hill, X. Chen, X. Wang, L. E. Mundt, K. H. Stone, L. T. Schelhas, G. Teeter, S. Parkin, E. L. Ratcliff, Y.-L. Loo, J. J. Berry, M. C. Beard, Y. Yan, B. W. Larson, K. Zhu, *Science* **2022**, *375*, 71–76; c) Y. H. Lin, N. Sakai, P. Da, J. Wu, H. C. Sansom, A. J. Ramadan, S. Mahesh, J. Liu, R. D. J. Oliver, J. Lim, L. Aspitarte, K. Sharma, P. K. Madhu, A. B. Morales-Vilches, P. K. Nayak, S. Bai, F. Gao, C. R. M. Grovenor, M. B. Johnston, J. G. Labram, J. R. Durrant, J. M. Ball, B. Wenger, B. Stannowski, H. J. Snaith, *Science* **2020**, *369*, 96–102.

[3] a) C. Luo, G. Zheng, F. Gao, X. Wang, C. Zhan, X. Gao, Q. Zhao, *Nat. Photonics* **2023**, *17*, 856–864; b) M. Ghasemi, B. Guo, K. Darabi, T. Wang, K. Wang, C. W. Huang, B. M. Lefler, L. Taussig, M. Chauhan, G. Baucom, T. Kim, E. D. Gomez, J. M. Atkin, S. Priya, A. Amassian, *Nat. Mater.* **2023**, *22*, 329–337; c) G. Wu, R. Liang, Z. Zhang, M. Ge, G. Sun, *Small* **2021**, *17*, 2103514.

[4] J. Haruyama, K. Sodeyama, L. Han, Y. Tateyama, *J. Am. Chem. Soc.* **2015**, *137*, 10048–10051.

[5] a) Z. Zhang, M. Li, R. Li, X. Zhuang, C. Wang, X. Shang, D. He, J. Chen, C. Chen, *Adv. Mater.* **2024**, *36*, 2313860; b) D. Wei, F. Ma, R. Wang, S. Dou, P. Cui, H. Huang, J. Ji, E. Jia, X. Jia, S. Sajid, A. M. Elseman, L. Chu, Y. Li, B. Jiang, J. Qiao, Y. Yuan, M. Li, *Adv. Mater.* **2018**, *30*, 1707583; c) J. Xu, P. Shi, K. Zhao, L. Yao, C. Deger, S. Wang, X. Zhang, S. Zhang, Y. Tian, X. Wang, J. Shen, C. Zhang, I. Yavuz, J. Xue, R. Wang, *ACS Energy Lett.* **2024**, *9*, 1073–1081; d) Y. Zhao, I. Yavuz, M. Wang, M. H. Weber, M. Xu, J. H. Lee, S. Tan, T. Huang, D. Meng, R. Wang, J. Xue, S. J. Lee, S. H. Bae, A. Zhang, S. G. Choi, Y. Yin, J. Liu, T. H. Han, Y. Shi, H. Ma, W. Yang, Q. Xing, Y. Zhou, P. Shi, S. Wang, E. Zhang, J. Bian, X. Pan, N. G. Park, J. W. Lee, Y. Yang, *Nat. Mater.* **2022**, *21*, 1396–

1402; e) Y. Yang, R. Chen, J. Wu, Z. Dai, C. Luo, Z. Fang, S. Wan, L. Chao, Z. Liu, H. Wang, *Angew. Chem. Int. Ed.* **2024**, 63, e202409689.
[6] J. Ding, L. Jing, X. Cheng, Y. Zhao, S. Du, X. Zhan, H. Cui, *J. Phys. Chem. Lett.* **2018**, *9*, 216–221.
[7] Z. Zuo, J. Ding, Y. Li, Y. Zhao, S. Du, *Mater. Res. Bull.* **2018**, *99*, 466–470.
[8] a) C. Ma, M. C. Kang, S. H. Lee, S. J. Kwon, H. W. Cha, C. W. Yang, N. G. Park, *Joule* **2022**, *6*, 2626–2643; b) D. Li, X. Sun, Y. Zhang, Z. Guan, Y. Yue, Q. Wang, L. Zhao, F. Liu, J. Wei, H. Li, *Adv. Sci.* **2024**, *11*, 2401184.
[9] C. Ma, F. T. Eickemeyer, S. H. Lee, D. H. Kang, S. J. Kwon, M. Grätzel, N. G. Park,*Science* **2023**, *379*, 173–178.
[10] a) X. Sun, D. Li, L. Zhao, Y. Zhang, Q. Hu, T. P. Russell, F. Liu, J. Wei, H. Li, *Adv. Mater.* **2023**, *35*, 2301115; b) G. Wu, R. Liang, M. Ge, G. Sun, Y. Zhang, G. Xing, *Adv. Mater.* **2022**, *34*, 2105635.
[11] X. Jiang, B. Liu, X. Wu, S. Zhang, D. Zhang, X. Wang, S. Gao, Z. Huang, H. Wang, B. Li, Z. Xiao, T. Chen, A. K.-Y. Jen, S. Xiao, S. Yang, Z. Zhu, *Adv. Mater.* **2024**, *36*, 2313524.
[12] a) B. Jiao, Y. Ye, L. T, Y. Liu, N. Ren, M. Li, J. Zhou, H. Li, Y. Chen, X. Li, C. Yi, *Adv. Mater.* **2024**, *36*, 2313673; b) Y. Yang, C. Liu, O. A. Syzgantseva, M. A. Syzgantseva, S. Ma, Y. Ding, M. Cai, X. Liu, S. Dai, M. K. Nazeeruddin, *Adv. Energy Mater.* **2021**, *11*, 2002966.
[13] H. Huang, P. Cui, Y. Chen, L. Yan, X. Yue, S. Qu, X. Wang, S. Du, B. Liu, Q. Zhang, Z. Lan, Y. Yang, J. Ji, X. Zhao, Y. Li, X. Wang, X. Ding, M. Li, *Joule* **2022**, *6*, 2186–2202.
[14] a) Y. Yuan, Q. Wang, Y. Shao, H. Lu, T. Li, A. Gruverman, J. Huang, *Adv. Energy Mater.* **2016**, *6*, 1501803; b) Y. Yuan, J. Chae, Y. Shao, Q. Wang, Z. Xiao, A. Centrone, J. Huang, *Adv. Energy Mater.* **2015**, *5*, 1500615; c) Y. Yang, Q. Chang, Y. Yang, Y. Jiang, Z. Dai, X. Huang, J. Huo, P. Gao, H. Shen, Z. Liu, R. Chen, H. Wang, *J. Mater. Chem. A.* **2023**, *11*, 16871.
[15] C. Jiang, J. Zhou, H. Li, L. Tan, M. Li, W. Tress, L. Ding, M. Grätzel, C. Yi,*Nano-Micro Lett.* **2023**, *15*, 12.
[16] a) S. Yuan, F. Lou, Y. Li, H. Y. Wang, Y. Wang, X. C. Ai, J. P. Zhang, *Appl. Phys. Lett.* **2023**, *122*, 133502; b) Y. Li, S. Yuan, S. Miao, J. Wu, H. Y. Wang, Y. Wang, X. C. Ai, J. P. Zhang, *J. Phys. Chem. C* **2023**, *127*, 14679–14686.
[17] R. Gottesman, P. Lopez-Varo, L. Gouda, J. A. Jimenez-Tejada, J. Hu, S. Tirosh, A. Zaban, J. Bisquert, *Chem* **2016**, *1*, 776–789.
[18] S. Yuan, H. Y. Wang, F. Lou, X. Wang, Y. Wang, Y. Qin, X. C. Ai, J. P. Zhang, *J. Phys. Chem. C* **2022**, *126*, 3696–3704.
[19] a) P. Cui, D. Wei, J. Ji, H. Huang, E. Jia, S. Dou, T. Wang, W. Wang, M. Li, *Nat. Energy* **2019**, *4*, 150–159; b) Y. Bai, Z. Huang, X. Zhang, J. Lu, X. Niu, Z. He, C. Zhu, M. Xiao, Q. Song, X. Wei, C. Wang, Z. Cui, J. Dou, Y. Chen, F. Pei, H. Zai, W. Wang, T. Song, P. An, J. Zhang, J. Dong, Y. Li, J. Shi, H. Jin, P. Chen, Y. Sun, Y. Li, H. Chen, Z. Wei, H. Zhou, Q. Chen, *Science* **2022**, *378*, 747–754.
[20] Y. Zhao, F. Ma, Z. Qu, S. Yu, T. Shen, H. X. Deng, X. Chu, X. Peng, Y. Yuan, X. Zhang, J. You, *Science* **2022**, *377*, 531–534.
[21] L. Yan, H. Huang, P. Cui, S. Du, Z. Lan, Y. Yang, S. Qu, X. Wang, Q. Zhang, B. Liu, X. Yue, X. Zhao, Y. Li, H. Li, J. Ji, M. Li, *Nat. Energy* **2023**, *8*, 1158–1167.

Manuscript received: August 20, 2024
Accepted manuscript online: September 17, 2024
Version of record online: ■■, ■■

Research Article

Perovskite Solar Cells

S. Qu, H. Huang, J. Wang, P. Cui, Y. Li, M. Wang, L. Li, F. Yang, C. Sun, Q. Zhang, P. Zhu, Y. Wang, M. Li* ____ **e202415949**

Revealing and Inhibiting the Facet-related Ion Migration for Efficient and Stable Perovskite Solar Cells

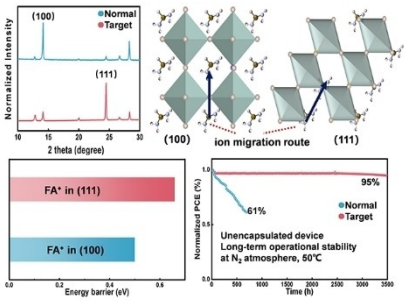

We first reveal the unknown relation between ion migration and crystal facet, in which the (100) facet is substantially more vulnerable to occur cationic migration than the (111) facet, and then control the (111)-orientation through an antisolvent strategy. The PSCs with (111)-dominated perovskite achieve a PCE of 26.0% (25.4% certification), and can maintain >95% of their initial PCEs after 3500-hours operation under 1-sun illumination.